Hindawi
Journal of Nanomaterials
Volume 2022, Article ID 8726662, 12 pages
https://doi.org/10.1155/2022/8726662

*Research Article*

# Self-Assembled PSMA-Targeted Nanoparticles Enhanced Photodynamic Therapy in Prostate Cancer

**Yongming Deng,[1] Qing Zhang,[2] Guangxiang Liu,[2] Tingsheng Lin,[2] Wenlong Zhang,[2] Xin He,[2] Wenfeng Lu,[2] Yuanzhen Ding,[2] Wenmin Cao,[2] and Hongqian Guo [1,2]**

[1]*Department of Urology, Nanjing Drum Tower Hospital Clinical College of Nanjing Medical University, 321 Zhongshan Road, Nanjing 210008, China*
[2]*Department of Urology, Drum Tower Hospital, Medical School of Nanjing University, Institute of Urology, Nanjing University, 321 Zhongshan Road, Nanjing, 210008 Jiangsu, China*

Correspondence should be addressed to Hongqian Guo; dr.ghq@nju.edu.cn

Received 4 August 2021; Revised 31 March 2022; Accepted 6 April 2022; Published 23 April 2022

Academic Editor: Donglu Shi



Prostate cancer greatly threatens human health. Many treatment strategies including surgery and radiotherapy are applied to treat prostate cancer. However, these treatment strategies will bring great side effects. Herein, we developed a functionalized Prostate-Specific Membrane Antigen-Chlorin e6 (PSMA-Ce6) NPs to enhance photodynamic therapy to reduce the side effects of prostate cancer treatments. We linked the hydrophobic photosensitizer Ce6 with the small hydrophilic molecule PSMA ligand through a covalent bond to form a functionalized PSMA-Ce6. In aqueous phase, the PSMA-Ce6 self-assembled into nanoparticles with a hydrophobic core and a hydrophilic shell, which significantly enhanced the accumulation of PSMA-Ce6 in the tumor. The molecularly targeted drug PSMA inhibitor can not only specifically inhibit PSMA but also increase the accumulation of the photosensitizer Ce6 in the tumor and achieve a completed tumor ablation under the near infrared (NIR) irradiation. PSMA-Ce6 NPs have great potential for translation into clinical applications.

## 1. Introduction

Prostate cancer is the most common cancer in men worldwide, and it is also one of the main causes of death in men [1]. Early localized prostate cancer can achieve satisfactory tumor control effects through surgery [2]. However, the surgical procedure may bring risks such as the risk of urinary incontinence and sexual dysfunction [3]. Besides, radiotherapy also brings risks such as bladder irritability and abnormal bowel function [4, 5]. Patients with advanced prostate cancer need to receive adjuvant treatments such as endocrine therapy and chemotherapy, but the vast majority of patients will progress to castration-resistant prostate cancer after this treatment [6]. The castration-resistant prostate cancer will face difficult conditions such as disease progression, shortened survival, and reduced quality of life [7]. Therefore, it is necessary to develop a novel therapeutic plan to improve the therapeutic efficacy and reduce the incidence of complications, thereby improving the quality of life of prostate cancer patients and prolonging the survival period.

Photodynamic therapy (PDT) is a new method for the treatment of tumors with laser-activated photosensitizers [8]. The photosensitizer absorbs energy and transfers it to oxygen under the irradiation of a specific wavelength of laser light to generate singlet oxygen ($^1O_2$), which directly mediates the killing of tumor cells [9]. Extensive studies have shown that photodynamic therapy can efficiently ablate tumors in a minimally invasive manner, induce antitumor immune responses, and improve patient compliance [10, 11]. However, most photosensitizers are hydrophobic, and free photosensitizers are prone to stacking quenching and are easily metabolized by biological organisms [12]. Besides, the photosensitizer alone has no tumor-targeting accumulation effect. These factors greatly limit the clinical application

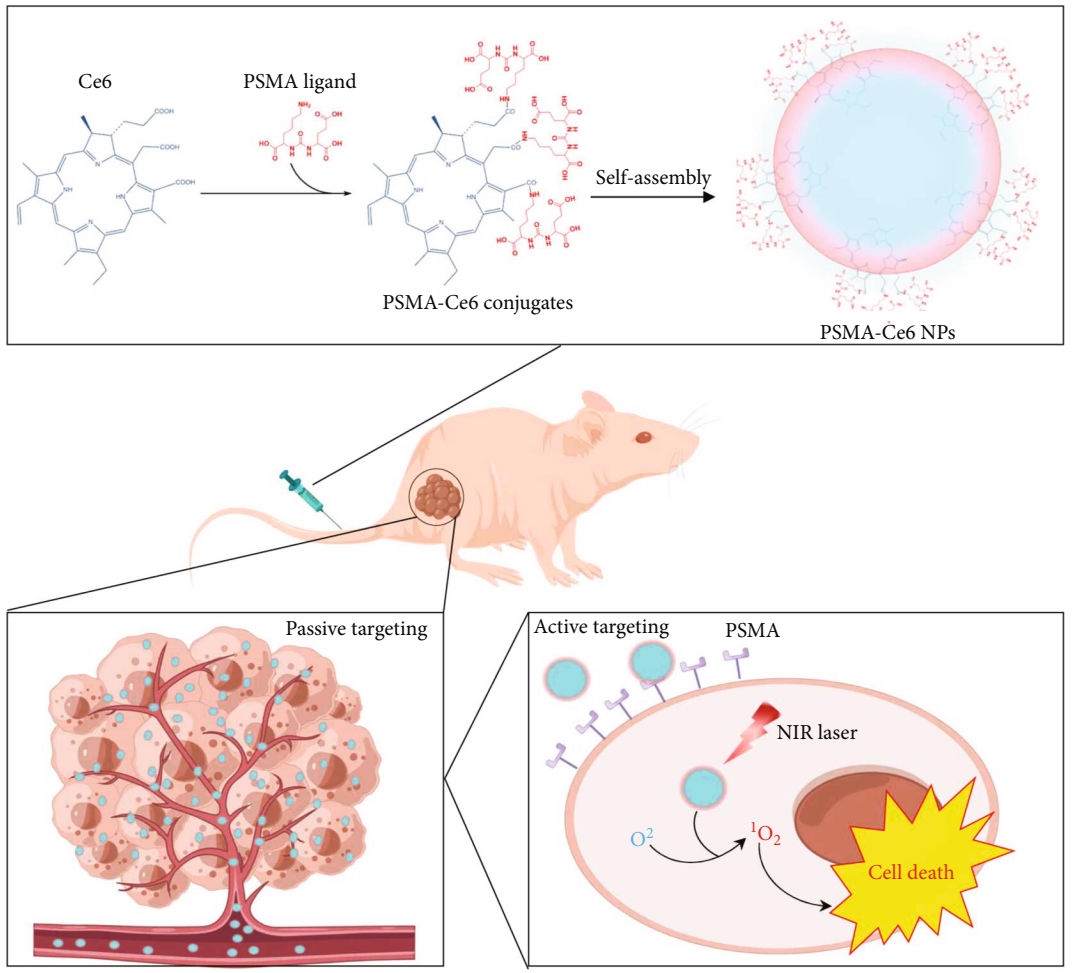


Scheme 1: Schematic illustration of preparation of PSMA-Ce6 and targeted to enhance photodynamic therapy in prostate cancer.

of photodynamic therapy [13]. Therefore, specific targeting of cancer cells to achieve targeted drug delivery has become a hot spot for photodynamic therapy.

Prostate-specific membrane antigen (PSMA) is a type II transmembrane protein that is highly expressed in most prostate cancer cells [14]. It is composed of 750 amino acid residues and has an internalization motif on its cytoplasmic side, which can trigger receptor-mediated endocytosis and internalize PSMA ligand-conjugated therapeutic drugs into cells [15]. PSMA is expressed at low levels in normal prostate tissue and hyperplastic prostate tissue. However, PSMA is highly expressed in prostate cancer cells and is closely related to poor prognosis such as castration resistance, recurrence, and metastasis [16]. PSMA has become a promising target for the diagnosis and treatment of prostate cancer, and radionuclide-labeled small-molecule PSMA inhibitors including $^{68}$Ga-PSMA and $^{177}$Lu-PSMA-617 have been widely used in clinical practice [17–19]. Therefore, coupling a photosensitizer and a molecular targeted medicine to form a nanoformulation can potentially enhance the accumulation of the drug in tumor cells, thereby achieving targeted photodynamic therapy.

In this study, we linked the hydrophobic photosensitizer Ce6 with the small hydrophilic molecule PSMA ligand through a covalent bond to form a functionalized PSMA-Ce6. In aqueous phase, the PSMA-Ce6 self-assembled into nanoparticles with a hydrophobic core and a hydrophilic shell, which significantly enhanced the accumulation of PSMA-Ce6 in the tumor (1). The molecularly targeted drug PSMA can not only specifically inhibit PSMA but also increase the accumulation of the photosensitizer Ce6 in the tumor. *In vivo* and *in vitro* human prostate cancer xenograft tumor models, PSMA-Ce6 NPs were injected into nude mice through the tail vein. In the case of NIR irradiation, singlet oxygen is generated, which synergistically inhibited PSMA to achieve complete tumor ablation, indicating that PSMA-Ce6 has an excellent tumor treatment effect.

## 2. Materials and Methods

*2.1. Chemical and Materials.* Chlorin e6 (Ce6) was purchased from Frontier Scientific (Logan, Utah, USA). N,N-dicyclohexylcarbodiimide (DCC), 4-dimethylaminopyridine (DMAP), and N,N-diisopropylethylamine (DEIA) were purchased from J&K Scientific Ltd. (China). 4′,6-diamidino-2-phenylindole dihydrochloride (DAPI) and Singlet Oxygen Sensor Green (SOSG) probe were from Molecular Probes (USA). The PSMA inhibitor (N-[[(5-amino-1-

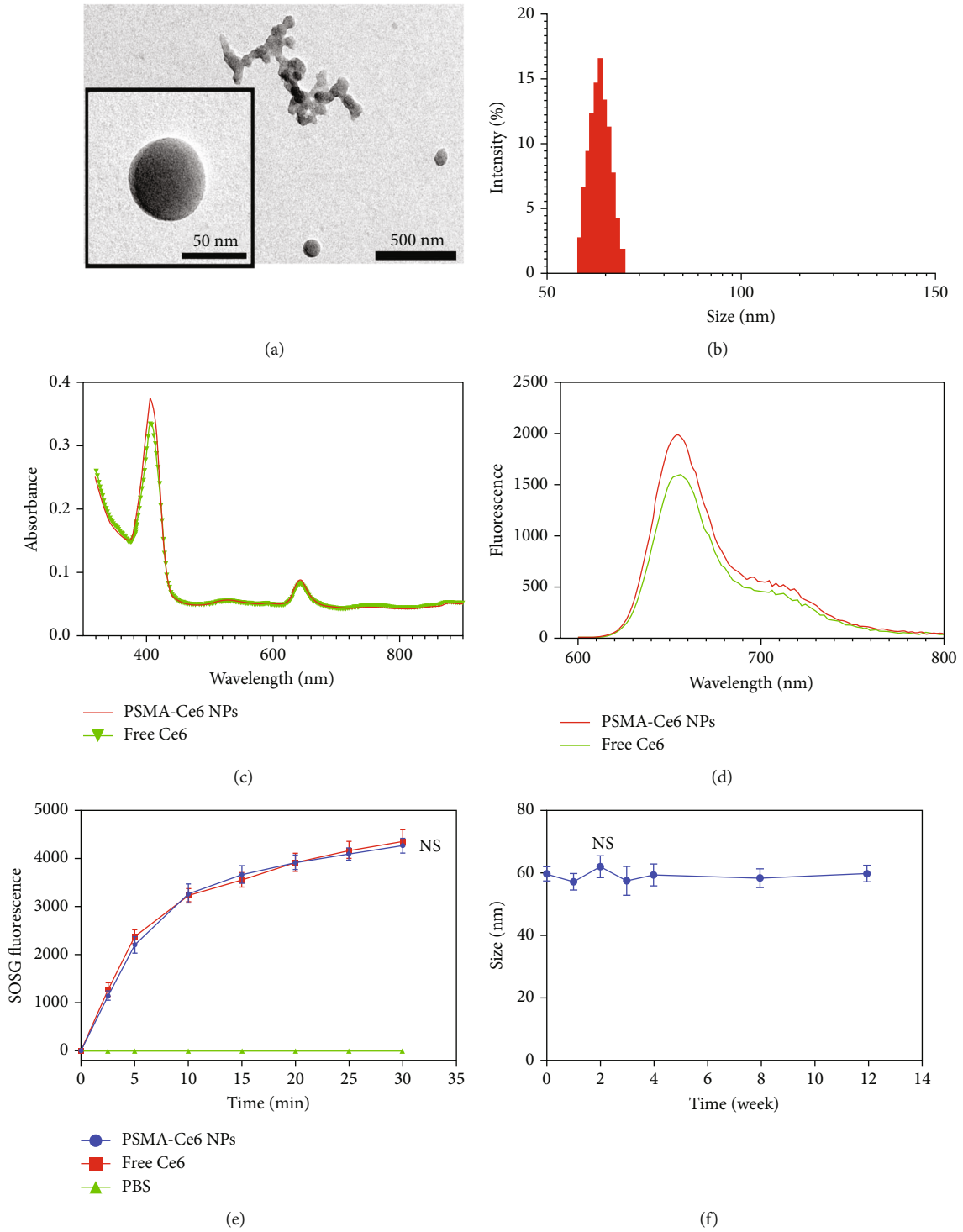


Figure 1: Characteristics of PSMA-Ce6 NPs. (a) Transmission electron microscope (TEM) imaging of PSMA-Ce6 NPs. (b) DLS particle size of PSMA-Ce6 NPs in deionized $H_2O$ ($n = 3$). (c) Normalized UV-vis spectra of free Ce6 and PSMA-Ce6 NPs. (d) Normalized fluorescence spectra of free Ce6 and PSMA-Ce6 NPs. (e) SOSG fluorescence intensity of free Ce6 and PSMA-Ce6 NPs ($n = 3$, $P > 0.05$ showed NS between these two groups). (f) DLS data of PSMA-Ce6 NPs incubated with saline at 37°C ($n = 3$, $P > 0.05$ showed NS within these weeks).

carboxypentyl) amino]carbonyl-Glutamic acid) was obtained from Nanjing Sunsure Chemical Technology Co., Ltd., the structure of this compound was confirmed by nuclear magnetic resonance hydrogen spectroscopy (1H-NMR) (Figure S1). Deionized water and 1 × phosphate buffer solution (PBS) were used throughout the experiments. 22RV1 and PC-3 cell lines were purchased from the Institute of Biochemistry and Cell Biology, Shanghai Institute of Life Sciences, Chinese Academy of Sciences. RPMI 1640 medium and 10% fetal bovine serum

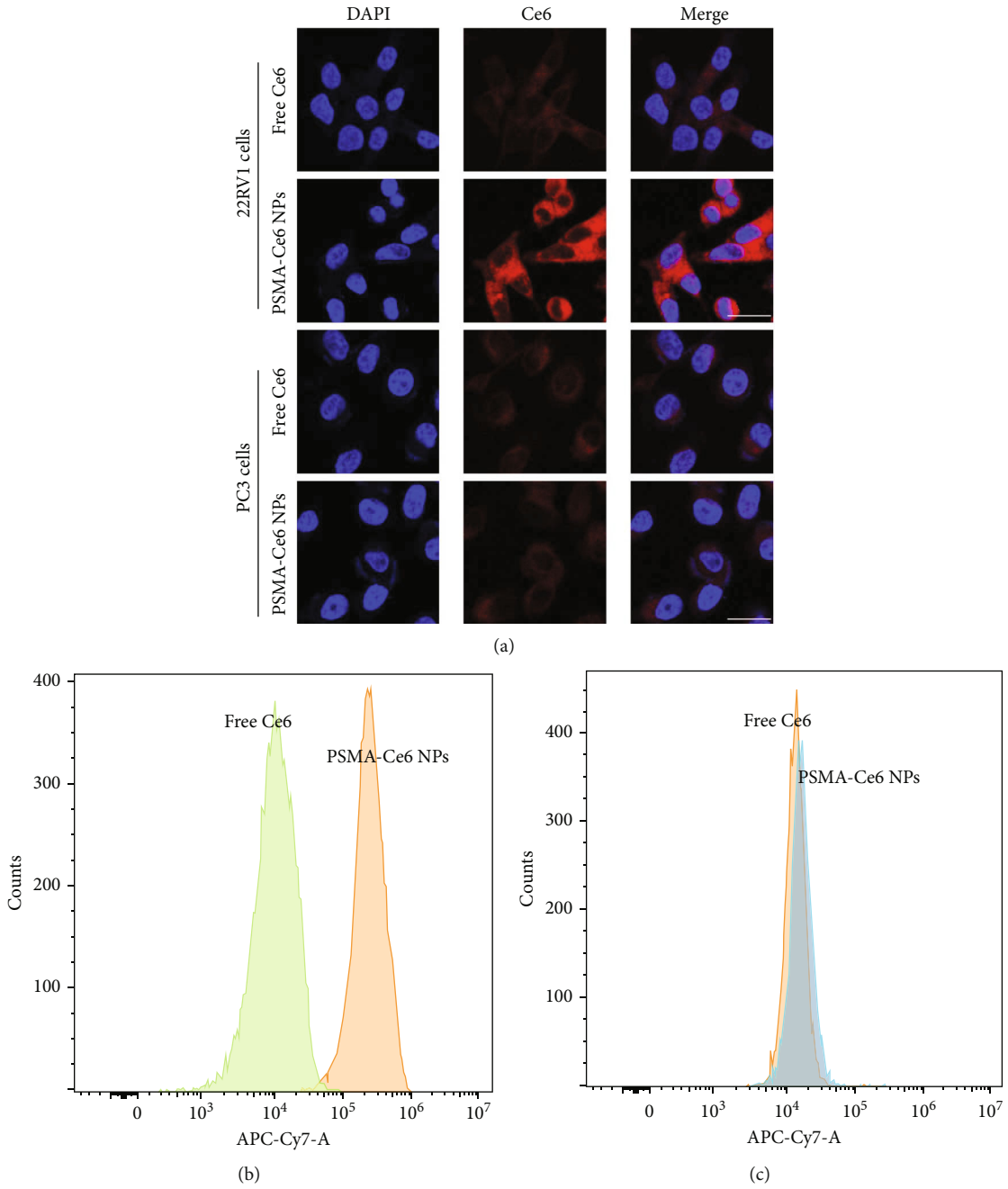


Figure 2: Cellular uptake of PSMA-Ce6 NPs. (a) Confocal laser scanning microscope (CLSM) images of 22Rv1 cells after treatment with DAPI and free Ce6 or PSMA-Ce6 NPs, respectively. Scale bar = 25 $\mu$m. (b) 22Rv1 cellular uptake behaviors of free Ce6 or PSMA-Ce6 NPs detected by flow cytometry ($n = 3$). (c) Confocal laser scanning microscope (CLSM) images of PC-3 cells after treatment with DAPI and free Ce6 or PSMA-Ce6 NPs, respectively. Scale bar = 25 $\mu$m. (d) PC-3 cellular uptake behaviors of free Ce6 or PSMA-Ce6 NPs detected by flow cytometry ($n = 3$).

(FBS) were purchased from Gibco (Grand Island, NY, USA). The BALB/c nude mice (male, 4-5 weeks, 18-20 g) were purchased from the Animal Core Facility of Nanjing Medical University. All animal studies were conducted according to the guidelines of the Institutional Animal Care and Use Committee of Nanjing Drum Tower Hospital.

*2.2. Synthesis of PSMA-Ce6.* First, chlorin e6 (100 mg, 0.168 mmol) dispersed in anhydrous dichloromethane (DCM, 10 mL) and N,N-diisopropylethylamine (DIEA, 0.06 mL, 0.34 mmol) was added. Then, N,N-dicyclohexylcarbodiimide (DCC, 105 mg, 0.51 mmol) and 4-dimethylaminopyridine (DMAP, 163 mg, 0.51 mmol) were dissolved in dichloromethane (DCM, 8 mL) and added to the reaction system with continuous stirring for 2 hours. Second, PSMA inhibitor (59.0 mg, 0.504 mmol) and N,N-diisopropylethylamine (DIEA, 0.075 mL) were dissolved in dichloromethane (DCM, 2 mL) and added to the reaction

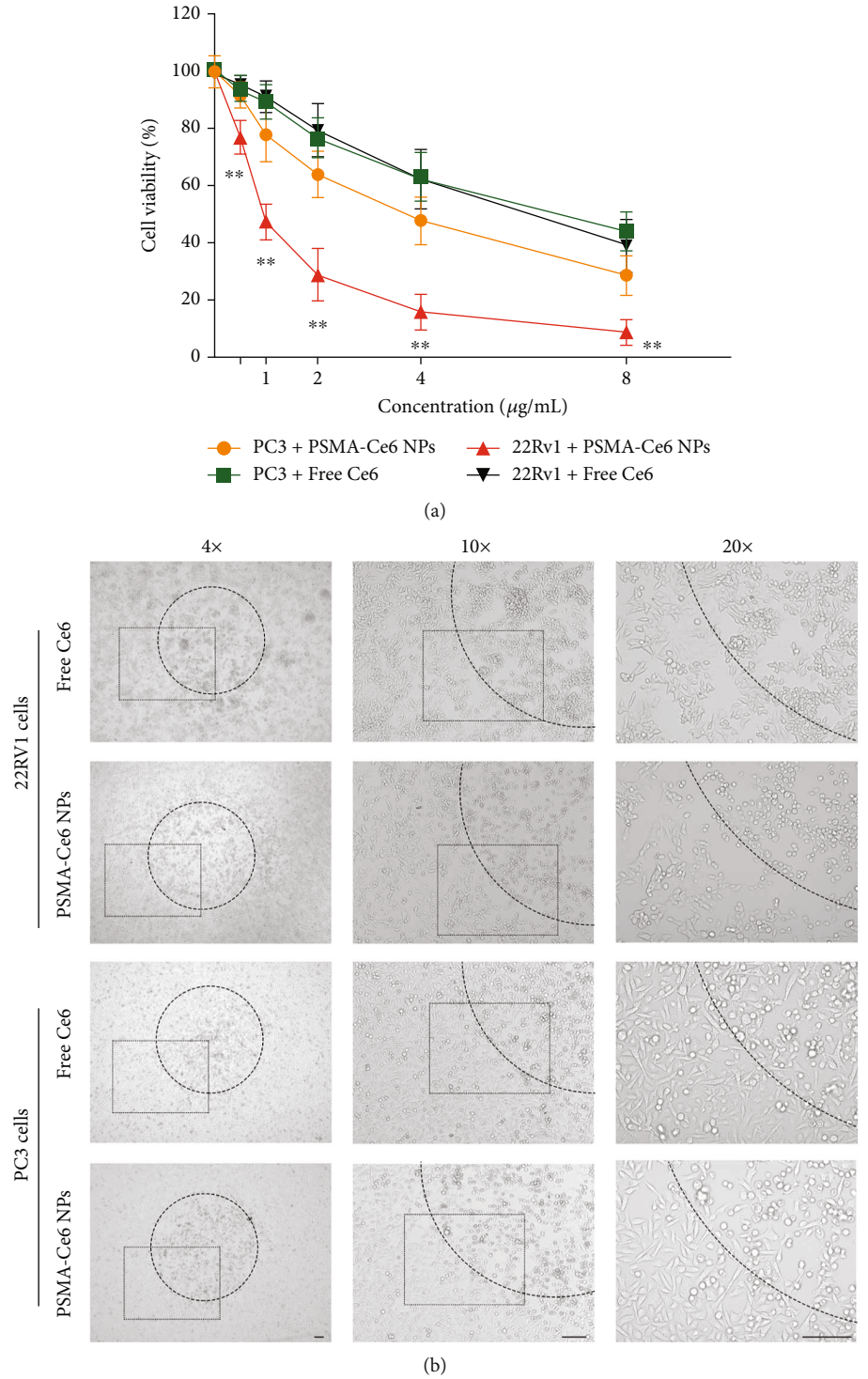


Figure 3: (a) *In vitro* cytotoxicity assay of PSMA-Ce6 NPs irradiated with a 660 nm near-infrared laser ($n = 3$, $**P < 0.01$, 22Rv1 with PSMA-Ce6 vs. other groups). (b) Photos of tumor cells after different treatments. The inner site and out site of dotted line represent treatments with and without laser irradiation, respectively. The square dotted line represents high magnifications of photos. Scale bar = 150 $\mu$m.

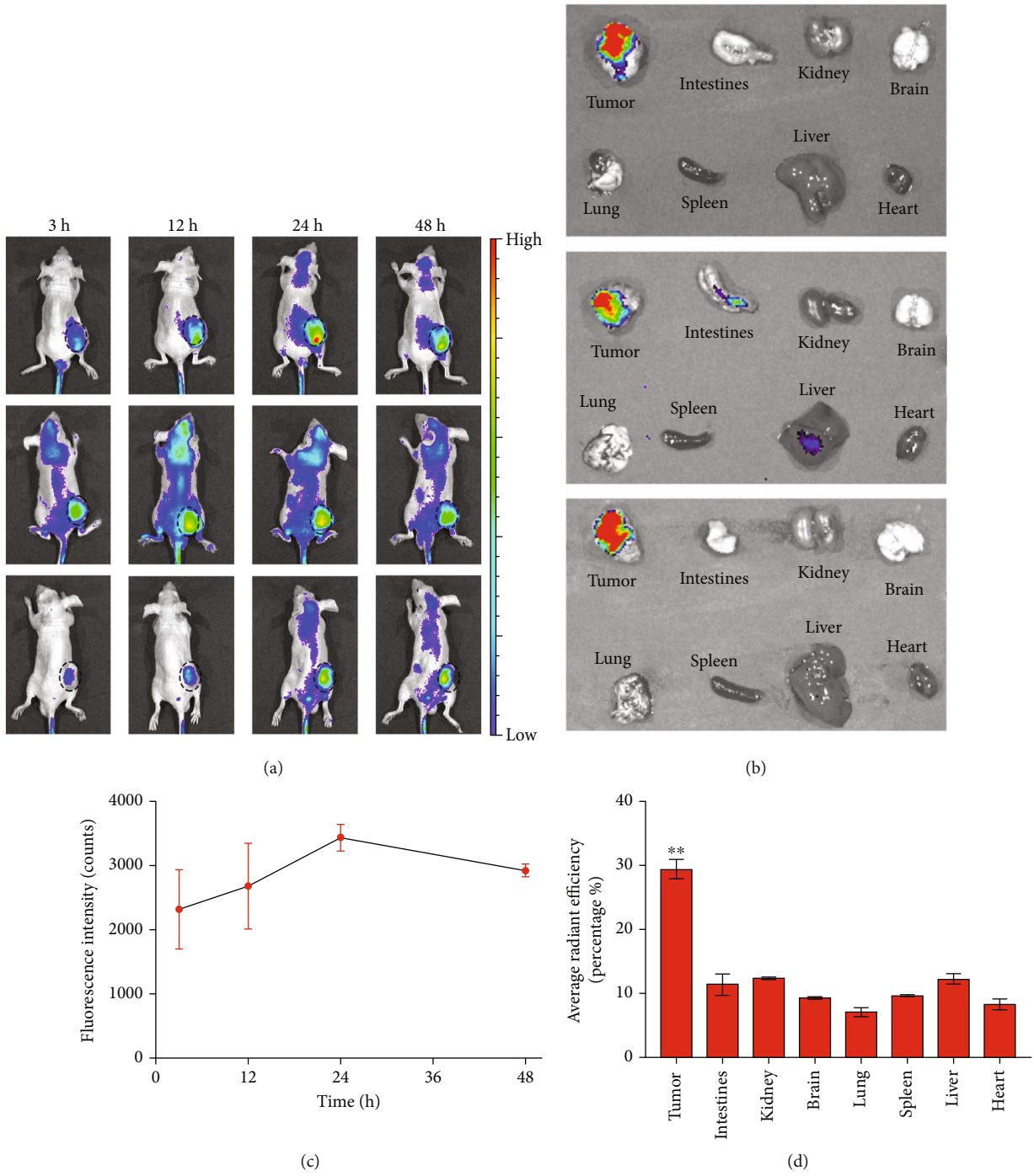


FIGURE 4: NIR imaging and biodistribution analysis. (a) *In vivo* dynamic fluorescence imaging after the tail vein injection of PSMA-Ce6 NPs at different time points. The dashed black circles indicated tumor regions. (b) Relative fluorescence intensity of primary tumor regions at various time points. (c) *Ex vivo* NIR fluorescence images of major organs and tumors at 48 hours postintravenous injection. (d) Ex vivo NIR fluorescence quantitation of major organs and tumors at 48 hours postintravenous injection ($n = 3$, $**P < 0.01$, tumor vs. other organs).

mixture with continuous stirring for another 24 hours at room temperature (r.t.). Allow the reaction to complete, dilute with DCM and wash with saturated physiological saline. After drying over anhydrous magnesium sulfate, the solvent was evaporated under reduced pressure. The residue was dissolved in 5% methanol/DCM and purified by silica gel column chromatography with methanol/DCM mobile phase to afford PSMA-Ce6. The structure of this compound was confirmed by $^1$H-NMR (Figure S2). The purified PSMA-Ce6 was dissolved in PBS, which was self-assembled to form PSMA-Ce6 NPs.

*2.3. Characterization of PSMA-Ce6 NPs.* The amount of PSMA-Ce6 was determined by ultraviolet-visible absorption

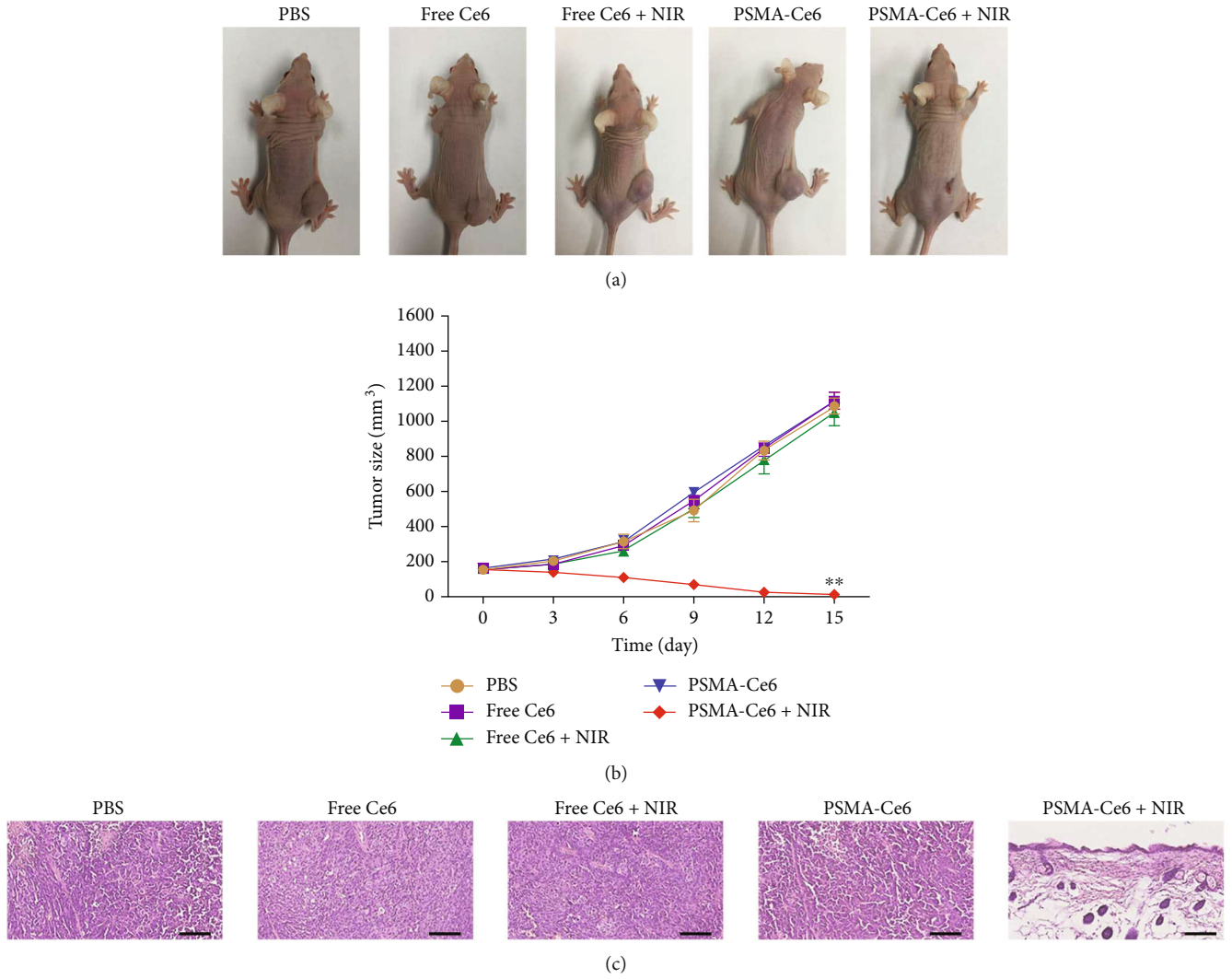


FIGURE 5: *In vivo* therapeutic effect of PSMA-Ce6 NPs. (a) Representative images of mice bearing prostate cancer after various treatments. (b) The tumor growth curves of different group of mice after various treatments indicated ($n = 5$, $**P < 0.01$, PSMA-Ce6 with NIR vs. other treatments). Error bars were based on standard errors of the mean. (c) The corresponding H&E-stained tumor sections. Scale bar = 250 $\mu$m.

spectroscopy (UV-Vis, UV2450, Shimadzu Corporation). The morphology and particle sizes of PSMA-Ce6 NPs were measured by transmission electron microscope (TEM) (Hitachi H-7650). The PSMA-Ce6 NPs are uniformly dispersed in 2.0 mL of deionized $H_2O$ (25°C), and then, the PSMA-Ce6 NPs solution was added to the cuvette and inserted with AQ-961 palladium electrode for zeta potential detection (Brookhaven 90 plus Zeta) [20]. The $^1O_2$ generation under laser irradiation by PSMA-Ce6 NPs was measured with an SOSG probe. In brief, SOSG dissolved in methanol was added to the samples to measure $^1O_2$ generation, which were irradiated with a 660-nm laser (5 mW cm$^{-2}$). The generated $^1O_2$ was determined by measuring recovered SOSG fluorescence at 525 nm under 494 nm excitation.

*2.4. In Vitro Cellular Uptake of PSMA-Ce6 NPs.* 22Rv1 cells and PC-3 cells were, respectively, seeded at a density of $1.0 \times 10^5$ cells per dish in confocal dishes (Coverglass Bottom Dish, dish size: 35 mm, hole size: 20 mm), respectively. A total of 4 groups ($n = 3$) were set up, including the 22Rv1 cell group with free Ce6, the 22Rv1 cell group with PSMA-Ce6 NPs, the PC-3 cell group with free Ce6, and the PC-3 cell group with PSMA-Ce6 NPs. The cells were given [Ce6] = 2 $\mu$g mL$^{-1}$ and incubated for 6 h after overnight attachment. The nucleus was stained with DAPI. The dishes were washed with PBS for three times, and cells were visualized under confocal laser scanning microscopy (Leica TCS SP5, Germany) to observe Ce6 fluorescence.

Then, 22Rv1 cells and PC-3 cells were cultured in six-well plates at a density of $1.0 \times 10^5$ cells per well in parallel. Administration of free Ce6 or PSMA-Ce6 NPs was performed at 3 h before 22Rv1 cells and PC-3 cells were harvested for further measurement by flow cytometry, respectively. Ce6 fluorescence was detected by APC-A channel.

*2.5. In Vitro Therapeutic Efficacy of PSMA-Ce6 NPs.* First, the hemolysis experiment of PSMA-Ce6 NPs was evaluated.

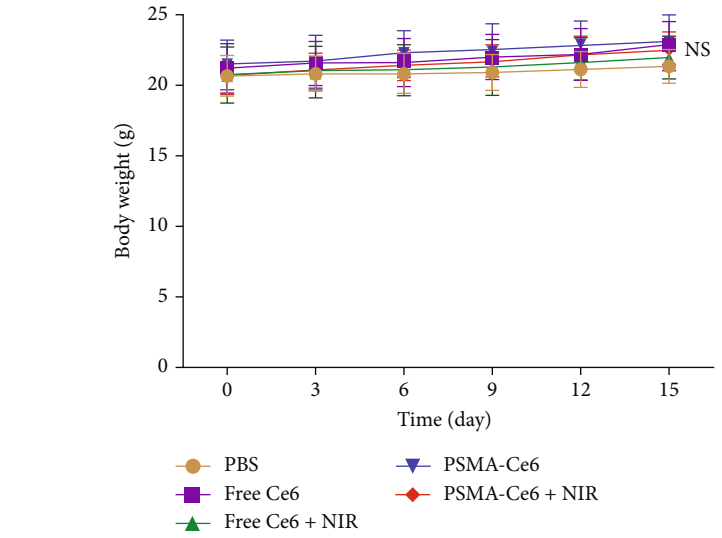


(a)

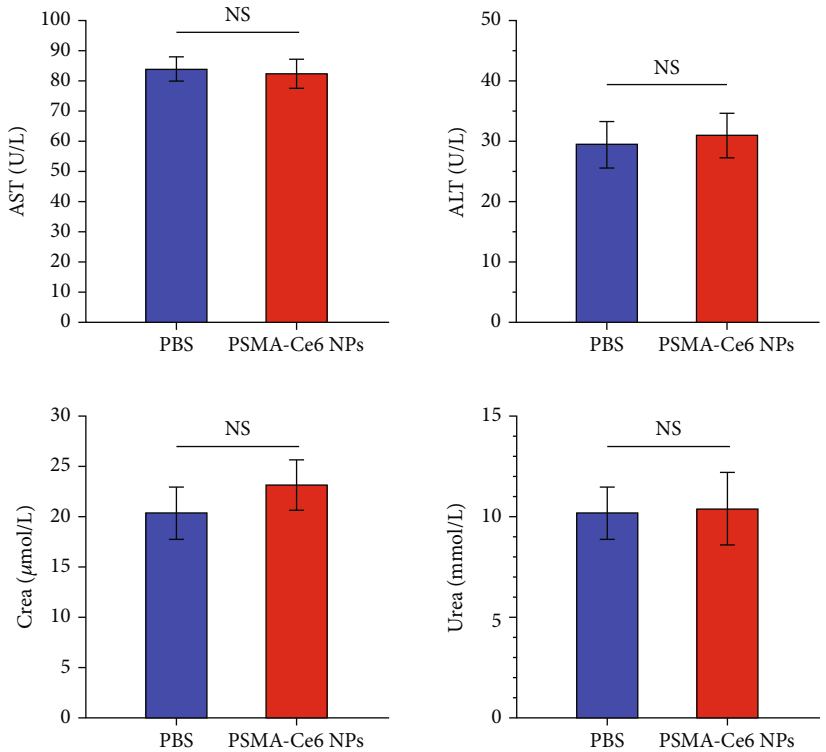


(b)

Figure 6: Continued.

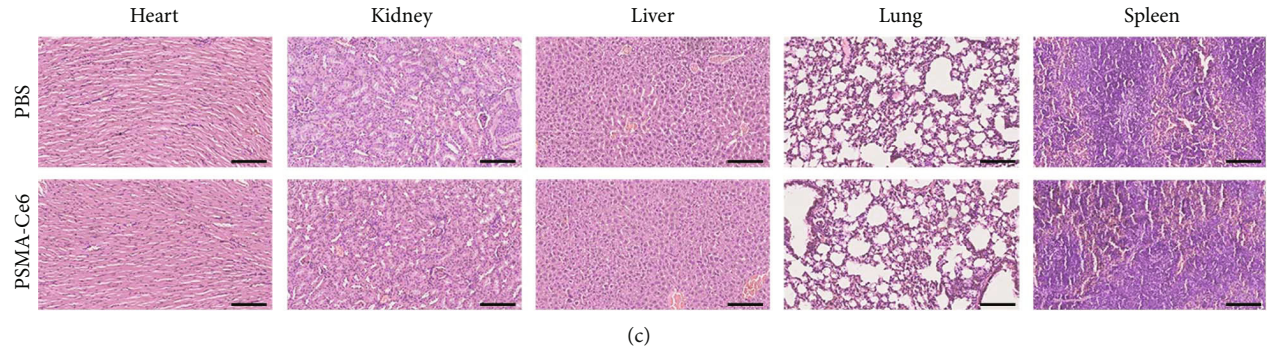


Figure 6: Biosafety evaluation of PSMA-Ce6 NPs *in vivo*. (a) Body weight of mice in different groups after various treatments ($n = 5$, $P > 0.05$ showed NS with these treatments). (b) Hepatic function evaluated by AST and ALT levels and renal function by CREA and UREA levels ($n = 5$, $P > 0.05$ showed NS with these treatments). (c) H&E staining of major organs (heart, kidney, liver, lung, and spleen) after the treatment of nanoparticles. Scale bar = 250 $\mu$m.

The blood was collected from *BALB/c* nude mice, and red blood cells were separated by centrifugation (500 g × 5 min) and then washed three times with PBS. The cells were treated with different concentrations of PSMA-Ce6 NPs ([Ce6] = 0, 5, 50, 100 $\mu$g mL$^{-1}$) and then centrifuged to detect the absorbance at 540 nm of the supernatant. The red blood cells are treated with 1% Triton-X 100 (Sigma-Aldrich) PBS solution as a standard for 100% hemolysis.

The cytotoxicity was evaluated with MTT assay (5 mg mL$^{-1}$, Dojindo Laboratories, Japan, 10 $\mu$L well$^{-1}$). To investigate the cytotoxicity of free Ce6 and PSMA-Ce6 NPs with 660 nm near-infrared laser (5 mW cm$^{-2}$, 30 min) irradiation, 22Rv1 cells and PC-3 cells were, respectively, seeded on 96-well plates at $5 \times 10^3$ well$^{-1}$ and further cultured for 12 h. Then, free Ce6 or PSMA-Ce6 NPs ([Ce6] = 0, 0.5, 1, 2, 4, and 8 $\mu$g mL$^{-1}$) were added and incubated for 12 h. After 660 nm near-infrared laser (5 mW cm$^{-2}$, 30 min) irradiation, 22Rv1 cells and PC-3 cells were cultured continuously for another 48 h (culture medium was refreshed every 24 h) before determining the cell viability by MTT assay. The photos of tumor cells after different treatments with or without NIR irradiation were captured by microscopy (Nikon, Tokyo, Japan).

*2.6. In Vivo NIR Fluorescence Imaging of PSMA-Ce6 NPs.* To evaluate the biodistribution of PSMA-Ce6 NPs *in vivo*, 22Rv1 tumor-bearing mice (~150mm$^3$, $n = 3$) were treated with PSMA-Ce6 NPs or free Ce6 ([Ce6] = 2.5 mg kg$^{-1}$) with intravenous injection. After intravenous injection of PSMA-Ce6 NPs or free Ce6, 22Rv1 tumor-bearing mice were, respectively, photographed at 0, 12, 24, and 48 h postadministration by *in vivo* fluorescence imaging system (IVIS Lumina XR III Spectrum, USA). All mice were sacrificed 48 hours after the intravenous injection. The major organs including the heart, liver, spleen, lung, brain, kidney, intestine, and tumor tissue were collected for imaging observation. The excitation wavelength was 675 nm, and the emission wavelength was 710 nm~900 nm. Semiquantitative analysis of these organs was performed with NIR irradiation analysis software Living Imaging 4.2.

*2.7. Therapeutic Efficacy of PSMA-Ce6 NPs In Vivo.* 22Rv1 tumor-bearing mice were divided into five groups once the tumors reached about 150 mm$^3$ and administrated with PBS, free Ce6 ([Ce6] = 2.5 mg kg$^{-1}$), PSMA-Ce6 NPs ([Ce6] = 2.5 mg kg$^{-1}$), free Ce6 + NIR ([Ce6] = 2.5 mg kg$^{-1}$, 660 nm laser, 200 mW cm$^{-2}$, 20 min), and PSMA-Ce6 NPs + NIR ([Ce6] = 2.5 mg kg$^{-1}$, 660 nm laser, 200 mW cm$^{-2}$, 20 min). The drug administration was performed on day 0. Near-infrared laser irradiation was given 24 h after the drug intravenous injection. Tumor size and body weight were monitored every 3 days, and the tumor volume was calculated according to the formula for volume of ellipsoid sphere: $V = (\text{width})^2 \times \text{length} \times \pi/6$ ($\approx \text{width}^2 \times \text{length}/^2$). The tumor tissues and slices of major organ including heart, liver, spleen, lung, and kidney were collected on day 15 after the treatments, fixed with 4% formalin, embedded in paraffin, and subsequently stained under the guidance of hematoxylin and eosin (H&E) standard protocol. The serum was also collected to determine serum biochemistry (UREA, CREA, AST, and ALT) on day 15 after the treatments. In order to further confirm the safety of PSMA-Ce6 NPs, after intravenous injection of PSMA-Ce6 NPs and PBS to nude mice, the serum of day 3 was also collected to determine serum biochemistry.

*2.8. Statistical Analysis.* Statistical analysis was performed by using two-tailed Student's $t$ test for two groups and one-way analysis of variance for multiple groups. $P$ values > 0.05 represented nonsignificance (N.S.). $*P$ values < 0.05 and $**P$ < 0.01 represented statistically significant.

## 3. Results and Discussion

*3.1. Preparation and Characterization of PSMA-Ce6 NPs.* Since PSMA-Ce6 are amphiphilic compounds, they will self-assemble into a hydrophobic core and a hydrophilic shell in an aqueous environment [21–23]. TEM imaging further confirmed their size and nanosphere morphology (Figure 1(a)). To support that the as-prepared PSMA-Ce6 is composed of a hydrophobic core and a hydrophilic shell. We next determined the contact angle of the PSMA-Ce6 in the aqueous phase, the contact angle of PSMA-Ce6 is about

21.8°, and this result indicates that the PSMA-Ce6 is wettable in the aqueous phase (Figure S3). Dynamic light scattering (DLS) data indicated that PSMA-Ce6 NPs exhibited an averaged diameter of 63.4 nm in deionized water, respectively (Figure 1(b)). The PSMA-Ce6 NPs showed negative surface charge, determined as $-18 \pm 2$ mv. Free Ce6 and PSMA-Ce6 NPs showed the same ultraviolet (UV) absorption peak at 408 nm and 660 nm, confirming the presence of Ce6 within PSMA-Ce6 NPs (Figure 1(c)). The fluorescence spectra of free Ce6 and PSMA-Ce6 NPs showed a strong fluorescence at 660 nm under the excitation wavelength of 408 nm (Figure 1(d)). Singlet oxygen ($^1O_2$) produced by PDT was the most vital cytotoxic radical species, which could be measured by SOSG probe. As shown in Figure 1(e), both free Ce6 and PSMA-Ce6 NPs could effectively produce abundant $^1O_2$ compared with PBS group under the 660 nm NIR. We further investigated the stability of PSMA-Ce6 NPs in saline at 37°C by DLS, indicating that PSMA-Ce6 NPs could keep stable within 12 weeks for further studies (Figure 1(f)).

*3.2. Intracellular Behaviors of PSMA-Ce6.* The cellular behavior of free Ce6 and PSMA-Ce6 NPs by prostate cancer cells 22Rv1 (PSMA expression positive) and PC-3 (PSMA expression negative) [24–26] was analyzed by confocal laser scanning microscope (CLSM). The CLSM images showed that after incubation with PSMA-Ce6 NPs, intense red fluorescence was observed in the cytoplasm of 22Rv1 cells, while less red fluorescence was found in the cytoplasm of 22Rv1 cells treated with free Ce6 (Figure 2(a)). The flow cytometric analysis further showed that PSMA-Ce6 NPs could be taken up by 22Rv1 cells and were significantly better than free Ce6 (Figure 2(b)). These results indicated that 22Rv1 cells can specifically take up PSMA-Ce6 NPs. However, in PC-3 cells with low expression of PSMA, there was no significant difference in red fluorescence between the cells treated with free Ce6 or PSMA-Ce6 NPs (Figure 2(c)). Flow cytometric analysis further confirmed that there was no significant advantage in the uptake of PSMA-Ce6 NPs by PC-3 cells compared with free Ce6 (Figure 2(d)). It shows that PC-3 cells with low expression of PSMA cannot take up PSMA-Ce6 NPs specifically. All results demonstrated that PSMA-Ce6 NPs can effectively target prostate cancer with high PSMA expression.

*3.3. In Vitro Assessment of the Photodynamic Effect of PSMA-Ce6 NPs against Prostate Cancer Cells.* Next, we examined the antitumor effects of free Ce6 and PSMA-Ce6 NPs in prostate cancer cells *in vitro*. The hemolysis experiment of PSMA-Ce6 NPs was first assessed, and we extracted *BALB/c* nude mice erythrocytes and added different concentrations of PSMA-Ce6 NPs to observe erythrocyte rupture. The results demonstrated that different concentrations of PSMA-Ce6 NPs did not cause significant hemolysis, indicating that PSMA-Ce6 NPs had good biocompatibility (Figure S4).

Then, the phototoxicity of PSMA-Ce6 NPs on prostate cancer cells was evaluated. PSMA-positive 22Rv1 prostate cancer cells were incubated with different concentrations of PSMA-Ce6NPs (0.5, 1.0, 2.0, 4.0, and 8.0 $\mu g\,mL^{-1}$ for [Ce6], respectively) and then irradiated with a 660 nm near-infrared laser, and cell viability was assessed by MTT cytotoxicity assay. As shown in Figure 3(a), PSMA-Ce6 NPs led to an increase in the cell death rate of 22Rv1 prostate cancer cells with increasing Ce6 concentration, and the cell viability decreased to less than 10% at Ce6 concentration of 8 $\mu g\,mL^{-1}$. In contrast, the killing effect of PSMA-Ce6 NPs under the same laser irradiation conditions was lower at all concentrations of treatment when co-incubated with PSMA-negative PC-3 cells. The killing effect of free Ce6 on prostate cancer cells was also very low and did not exhibit PSMA dependence. In addition, as shown in Figure S5, without laser irradiation, there showed no significant inhibition on 22Rv1 and PC-3 cells after incubation with PSMA-Ce6 and free Ce6. The photos of tumor cells include high and low magnifications were shown in Figure 3(b), which is consistent with the cell viability determined by MTT. In summary, PSMA-Ce6NPs can be actively taken up by 22Rv1 cells to exert photodynamic killing of prostate cancer cells, while PC-3 cells cannot actively take up PSMA-Ce6 NPs.

*3.4. In Vivo Fluorescence Imaging of PSMA-Ce6 NPs.* We next investigated the biodistribution of PSMA-Ce6 NPs in tumor-bearing mice by *in vivo* fluorescence imaging system (IVIS spectrum). The imaging observations were performed after tail vein injection of PSMA-Ce6 NPs into tumor-bearing mice, respectively. The results showed that the NIR fluorescence tendency of Ce6 accumulated in the subcutaneous xenograft tumors on the back of mice (the area indicated by the black dashed circle) and reached the accumulation peak after 24 h of administration (Figures 4(a) and 4(b)). Near-infrared imaging of various major organs removed after 48 hours of intravenous administration showed that the tumors had strong Ce6 near-infrared fluorescence accumulation, while other vital organs had little Ce6 accumulation (Figures 4(c) and 4(d)). These experimental results demonstrated that the PSMA-Ce6 NPs were tumor-targeted.

*3.5. In Vivo Therapeutic Effect of PSMA-Ce6 NPs.* Given that PSMA-Ce6 NPs can specifically accumulate in PSMA-positive prostate cancer cells, we subsequently assessed the *in vivo* antitumor effects of PSMA-Ce6 NPs at 22Rv1 subcutaneous xenograft mouse model. When the volume of 22Rv1 subcutaneous xenografts reached about 150 $mm^3$, we divided the mice randomly into five groups, which were PBS group, free Ce6, laser-irradiated free Ce6, PSMA-Ce6 NPs, and laser-irradiated PSMA-Ce6 NPs. Twenty-four hours after tail vein injection, the tumors of mice in the laser-irradiated group were exposed to laser irradiation at 660 nm. The results suggested that the tumor volume of mice in the PSMA-Ce6 NPs group with laser irradiation was significantly reduced, while the tumor volume of mice in the free Ce6 group with laser irradiation did not show obvious tumor suppression effect. These results indicated that PSMA-Ce6 NPs accumulated in the tumor and could exert photodynamic effects to kill tumor cells until scar

formation. However, the growth of transplanted tumors in mice in the free Ce6 group or PSMA-Ce6 NPs without laser irradiation hardly showed tumor suppression effect compared with the PBS group (Figures 5(a) and 5(b)). The results indicated that free Ce6 and PSMA-Ce6 NPs had no inhibitory effect on tumor cells growth. Besides, the H&E staining of tumor tissues further confirmed that PSMA-Ce6 NPs mediated photodynamic therapy induced extensive cell death (Figure 5(c)).

*3.6. In Vivo Safety Evaluation of PSMA-Ce6 NPs.* To evaluate the potential biological toxicity of PSMA-Ce6 NPs, we collected the body weight of mice and found that there was no significant difference in the body weight of mice among the treatment groups (Figure 6(a)). We further analyzed the serum biochemistry including UREA, CREA, ALT, and AST levels (Figure 6(b)) and H&E sections of major organs (Figure 6(c)) on day 15 after the treatment groups. In addition, the serum biochemistry on day 3 after intravenous injection was also evaluated, as shown in Figure S6. There was no significant difference after intravenous injection of PBS and PSMA-Ce6. These results indicated that there was no significant difference in liver and kidney function between the groups, and there was no significant pathological change in the structure of main organs (inflammation, edema, hyperplasia or necrosis, etc.). In conclusion, PSMA-Ce6 NPs have good biocompatibility with less side effects and good *in vivo* therapeutic biosafety.

## 4. Conclusion

In summary, using the hydrophobicity of Ce6 and the hydrophilicity of PSMA ligand, we linked the Ce6 with PSMA ligand through a covalent bond to form a functionalized PSMA-Ce6 NPs. These new PSMA-Ce6 NPs can specifically target prostate cancer cells and contribute to imaging diagnosis and specific treatment of prostate cancer. PSMA-Ce6 NPs have great potential for translation into clinical applications. PSMA-Ce6 NPs target prostate cancer cells through PSMA ligand on the surface, and then Ce6 fluorescence imaging can accurately indicate the location of the tumor, which can eventually exert photodynamic therapy under near-infrared laser irradiation. It is hoped that this image-guided PDT treatment of prostate cancer brings new ideas.

## Data Availability

The data used to support the findings of this study are included within the supplementary information file(s). Some other data used to support the findings of this study are currently under embargo while the research findings are commercialized. Requests for data, [6/12 months] after publication of this article, will be considered by the corresponding author.

## Conflicts of Interest

The authors declare no competing financial interest.

## Authors' Contributions

Yongming Deng, Qing Zhang, and Guangxiang Liu contributed equally to this work.

## Acknowledgments

We acknowledge the National Science Foundation of China (NSFC) (nos. 81972388, 81802532, and 81772710), the Project of Invigorating Health Care through Science, Technology and Education, Jiangsu Provincial Key Medical Discipline (Laboratory) (ZDXKB2016014), and the "Summit of the Six Top Talents" Program of Jiangsu Province (SWYY-084).

## Supplementary Materials

Figure S1: the nuclear magnetic resonance hydrogen spectroscopy ($^1$H-NMR) of the PSMA inhibitor. Figure S2: the nuclear magnetic resonance hydrogen spectroscopy ($^1$H-NMR) of the PSMA-Ce6. Figure S3: contact angle of the PSMA-Ce6 in the aqueous phase. Figure S4: hemolysis evaluation of PSMA-Ce6 NPs ($n = 3$ biologically independent cells) hemolysis ratio in different treatment groups, red blood cells treated with 1% TritonX100 (Sigma) in PBS served as 100% hemolysis criteria. Figure S5: in vitro cytotoxicity assay of PSMA-Ce6 NPs and free Ce6 in both PC3 and 22Rv1 without laser irradiation. Figure S6: hepatic function evaluated by AST and ALT levels and renal function by CREA and UREA levels on day 3 after intravenous injection of PBS and PSMA-Ce6 ($n = 5$, $P > 0.05$ showed NS with these treatments). *(Supplementary Materials)*

## References

[1] H. E. Taitt, "Global trends and prostate cancer: a review of incidence, detection, and mortality as influenced by race, ethnicity, and geographic l*ocation*," *Health*, vol. 12, no. 6, pp. 1807–1823, 2018.

[2] R. M. Hoffman, W. C. Hunt, F. D. Gilliland, R. A. Stephenson, and A. L. Potosky, "Patient satisfaction with treatment decisions for clinically localized prostate carcinoma. Results from the prostate cancer outcomes study," *Cancer*, vol. 97, no. 7, pp. 1653–1662, 2003.

[3] K. Robert, "Incidence of complications other than urinary incontinence or erectile dysfunction after radical prostatectomy or radiotherapy for prostate cancer: a population-based cohort study," *The Lancet Oncology*, vol. 15, no. 2, pp. 223–231, 2014.

[4] K. Blomberg, Y. Wengström, K. Sundberg et al., "Symptoms and self-care strategies during and six months after radiotherapy for prostate cancer - scoping the perspectives of patients, professionals and literature," *European Journal of Oncology Nursing*, vol. 21, pp. 139–145, 2016.

[5] Z. Huang, Y. Wang, D. Yao, J. Wu, Y. Hu, and A. Yuan, "Nanoscale coordination polymers induce immunogenic cell death by amplifying radiation therapy mediated oxidative stress," *Nature Communications*, vol. 12, no. 1, p. 145, 2021.

[6] N. Kim, "Castration-resistant prostate cancer: from new pathophysiology to new treatment targets," *European Urology*, vol. 56, no. 4, pp. 594–605, 2009.

[7] D. Lorente, J. Mateo, R. Perez-Lopez, J. S. de Bono, and G. Attard, "Sequencing of agents in castration-resistant prostate cancer," *The Lancet Oncology*, vol. 16, no. 6, pp. e279–e292, 2015.

[8] M. A. Awan and S. A. Tarin, "Review of photodynamic therapy," *The Surgeon*, vol. 4, no. 4, pp. 231–236, 2006.

[9] T. Gheewala, T. Skwor, and G. Munirathinam, "Photosensitizers in prostate cancer therapy," *Oncotarget*, vol. 8, no. 18, pp. 30524–30538, 2017.

[10] V. Straten, Demian, V. Mashayekhi et al., "Oncologic photodynamic therapy: basic principles, current clinical status and future directions," *Cancers*, vol. 9, no. 12, p. 19, 2017.

[11] R. R. Allison, "Photodynamic therapy: oncologic horizons," *Future Oncology*, vol. 10, no. 1, pp. 123-124, 2014.

[12] X. Li, S. Lee, and J. Yoon, "Supramolecular photosensitizers rejuvenate photodynamic therapy," *Chemical Society Reviews*, vol. 47, no. 4, pp. 1174–1188, 2018.

[13] R. Ron, "Photosensitizers in clinical PDT," *Photodiagnosis and Photodynamic Therapy*, vol. 1, no. 1, pp. 27–42, 2004.

[14] S. S. Chang, P. B. Gaudin, V. E. Reuter, D. S. O'Keefe, D. J. Bacich, and W. D. Heston, "Prostate-specific membrane antigen: much more than a prostate cancer marker," *Molecular Urology*, vol. 3, no. 3, pp. 313–320, 1999.

[15] S. S. Chang, "Overview of prostate-specific membrane antigen," *Revista de Urología*, vol. 6, pp. S13–S18, 2004.

[16] S. Mannweiler, P. Amersdorfer, S. Trajanoski, J. A. Terrett, D. King, and G. Mehes, "Heterogeneity of prostate-specific membrane antigen (PSMA) expression in prostate carcinoma with distant metastasis," *Pathology Oncology Research*, vol. 15, no. 2, pp. 167–172, 2009.

[17] C. A. Umbricht, M. Benešová, R. M. Schmid et al., "$^{44}$Sc-PSMA-617 for radiotheragnostics in tandem with $^{177}$Lu-PSMA-617-preclinical investigations in comparison with $^{68}$Ga-PSMA-11 and $^{68}$Ga-PSMA-617," *EJNMMI Research*, vol. 7, no. 1, p. 9, 2017.

[18] C. Kratochwil, F. L. Giesel, M. Stefanova et al., "PSMA-targeted radionuclide therapy of metastatic castration-resistant prostate cancer with177Lu-labeled PSMA-617," *Journal of Nuclear Medicine*, vol. 57, no. 8, pp. 1170–1176, 2016.

[19] Z. Huang, D. Yao, Q. Ye et al., "Zoledronic acid-gadolinium coordination polymer nanorods for improved tumor radioimmunotherapy by synergetically inducing immunogenic cell death and reprogramming the immunosuppressive microenvironment," *ACS Nano*, vol. 15, no. 5, pp. 8450–8465, 2021.

[20] B. D. Chen, W. Y. L. Le WJ, Z. Q. Li et al., "Targeting negative surface charges of cancer cells by multifunctional nanoprobes," *Theranostics*, vol. 6, no. 11, pp. 1887–1898, 2016.

[21] X. Q. Li, H. Y. Wen, H. Q. Dong et al., "Self-assembling nanomicelles of a novel camptothecin prodrug engineered with a redox-responsive release mechanism," *Chemical Communications*, vol. 47, no. 30, pp. 8647–8649, 2011.

[22] J. Ma, H. Dong, H. Zhu, C. W. Li, Y. Li, and D. shi, "Deposition of gadolinium onto the shell structure of micelles for integrated magnetic resonance imaging and robust drug delivery systems," *Journal of Materials Chemistry B*, vol. 4, no. 36, pp. 6094–6102, 2016.

[23] T. Lin, A. Yuan, X. Zhao et al., "Self-assembled tumor-targeting hyaluronic acid nanoparticles for photothermal ablation in orthotopic bladder cancer," *Acta Biomaterialia*, vol. 53, pp. 427–438, 2017.

[24] C. A. S. Regino, K. J. Wong, D. E. Milenic et al., "Preclinical evaluation of a monoclonal antibody (3C6) specific for prostate-specific membrane antigen," *Current Radiopharmaceuticals*, vol. 2, no. 1, pp. 9–17, 2009.

[25] Y. Gao, Y. Li, Y. Li et al., "PSMA-mediated endosome escape-accelerating polymeric micelles for targeted therapy of prostate cancer and the real time tracing of their intracellular trafficking," *Nanoscale*, vol. 7, no. 2, pp. 597–612, 2015.

[26] J. P. Dassie, X. Liu, G. S. Thomas et al., "Systemic administration of optimized aptamer-siRNA chimeras promotes regression of PSMA-expressing tumors," *Nature Biotechnology*, vol. 27, no. 9, pp. 839–846, 2009.